NTNU

Norwegian University of
Science and Technology

An Integrated Sub-nW CMOS Temperature Sensor for Realtime Thermal Monitoring of an Ultrasonic Probe

Submitted by: Dewan Abu Md Arefin
Supervised by: Trond Ytterdal

2020/08/24

Abstract

This report is about designing and implementing an on-chip lower power and area temperature sensor for an ultrasonic probe. The sensor was designed, implemented in schematic and simulated using the Virtuoso software for analysis and verification. The design of the circuit is based on another published paper [24], but with more smaller transistor dimensions in 90 nm CMOS technology. The sensor works in the sub-threshold region with only 600 mV of power supply. It operates over the temperature range of 0-120 °C, with maximum pulled current of 218.66 nA and mere power consumption of 131.2 nW at the highest temperature of 120 °C. It has an inaccuracy range of -3.3 to +7.6 °C with very high linearity and stability performance. It is based on measuring the temperature using the differences in gate-source voltages of a MOSFET which is proportional to the temperature in the sub-threshold region.

Acknowledgment

First of all I am very thankful to my supervisor Trond Ytterdal for his immense patience, guidance and help. Without him this project was not possible to be accomplished. His dedicated time and suggestion were very important to be able to make this project function properly. It was very interesting to work and play with the transistors and get a chance to know them better. Analog designing was sometimes depressing but at the same time it was new and fun thing to do. Along this journey I got to learn new things about analog designing and got a chance to hold a good grip on it.

Contents

Figures

Tables

Chapter 1

Introduction

Ultrasonic imaging technology plays a vital role in the field of medical science which has advanced immensely. It has made diagnosis processes easier, better, safer and readily available for everyone in the current world. A ultrasonic transducer, also called a probe, is the main component of ultrasound imaging system. This paper is focused on designing an integrated CMOS temperature sensor with low power, area and cost for the ultrasonic transducer. The temperature sensor is designed in 90 nm CMOS process with sub-threshold MOS operation which draws maximum current of 218.66 nA at the highest temperature of 120 °C with a supply voltage of 600 mV which result in maximum power consumption of 131.2 nW. The sensor has an inaccuracy of -3.3 to +7.6 °C for temperature range from 0 to 120 °C. Apart from medical devices, this temperature sensor can also be used in many other applications where maintaining a certain range of temperature is necessary such as automobile, aerospace, agriculture, industrial, computers, appliances and many other types of machinery.

1.1 Overview and Motivation

Some portion of the background information and knowledge needed for this design work were acquired in the project prior to this thesis [1] .Also, that preceding project has some contribution in the motivation for this master thesis work. This is revised with more discussion from a few number of papers which have been studied and materials from some other authentic sources. The presentation from the project report is given below in the following two paragraphs.

Over the past several years, ultrasound imaging has been adopted as one of the most crucial technique for medical analysis and diagnostic tests. It is favored over the traditionally established methods such as X-Rays, CAT scans

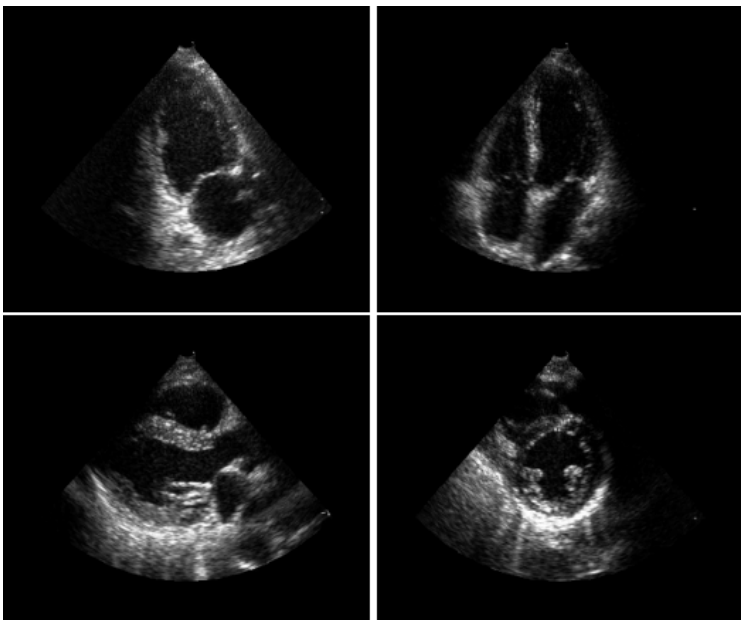

Figure 1.1: Four different ultrasound views of the heart. Clockwise from upper left: apical two chamber view, apical four chamber view, parasternal long axis view, and parasternal short axis view.[2]

and MRI due to its real time capabilities, cost effectiveness and safety. Ultrasound waves are non-invasive, does not use ionizing radiation and can generate real time 3D/4D images with high frames rates. Such characteristics enable the precise examination of the development of a fetus as well as brain and hips of infants, and moving tissues of a beating heart along with assessing the damage after a heart attack. One of such image is shown as example in figure 1.1. This made it the interesting technology of choice in the fields of obstetrics and cardiology respectively. Its other uses include the diagnosis for the causes of infection, pain and swelling in the internal organs of the body and they also assist and guide in carrying certain types of biopsy.

Sound waves are used in ultrasound imaging for producing images of what is going on the inside of the body. During an ultrasound test, the patient is lay on a table, a gel is applied to prevent the formation of air pockets which can block the sound waves that creates the images and a specialized person moves a device called transducer over the body parts. Sometimes, the transducer is attached to a probe which is inserted into the body through a natural opening. One example could be a transducer inserted into the esophagus while sedated which obtains the image of the heart. A transducer is a device which is used to generate ultrasound waves, being able to emit the ultrasound waves and detect the ones which are reflected back. The information from the reflected waves

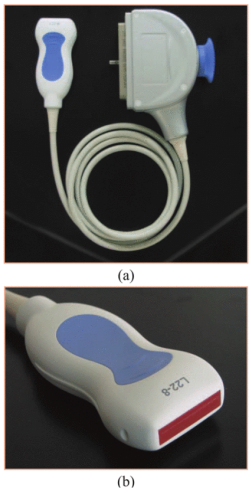

Figure 1.2: Picture of (a) L22-8 CMUT probe and (b) a probe scanhead.[3]

such as speed of sound, time to return of each echoed wave, and the distance of the transducer from the tissue boundary is used by a scanner and processor to produce three dimensional real time images of tissues and organs. Then finally the doctor examines and interprets the images in order to diagnose and treat certain conditions. One such CMUT probe and a probe scanhead is shown in the figure 1.2.

As there are many types of probes, some are either placed over the skin of and others are inserted inside the human body for scanning purposes. Therefore, it becomes one of the very crucial point to monitor the heat dissipation or temperature of this probe. This is required for the safety of both the patient as well as the device. Otherwise, overheating may take place causing harm to the skin or internal organs of the human body and even damaging the probe, both of them are quite expensive. Moreover, maintaining a specific temperature is very important once again for both the patient and as well as the device. The device has to operate in a certain specified range of temperature for proper functioning and monitoring of the patient. The accuracy and responsiveness of the device is also crucial for the diagnosis of the patient which may also collapse if this temperature range is exceeded. Even if it can be known whether the probe is too hot or too cold and the correct prevention steps could be taken in order to ensure the safety of both the device and the patients without risking the life of both.

Since most of the physical, biological, chemical, mechanical and electronic systems are effected by temperature, there is no doubt that it is of the most often measured environmental quantity. As it is one of the most commonly assessed variable and hence therefore it is not surprising that that there are many ways to do this. An electronic circuit in addition with certain biolo-

gical processes and chemical reactions performs well only in a specific temperature range. Here comes the use of temperature sensors and there are many ways of sensing the temperature. The temperature could be sensed directly by contact with the source or remotely from the radiated heat of the source. The wide variety of temperature sensors includes thermocouples. resistance temperature detectors (RTD), thermistors,infrared and semiconductor (CMOS or Bi-Polar) sensors. A vital role is often played by temperature sensors in many applications. Even though it is also required in the applications where temperature itself is not the main issue rather other components might not function properly if certain range of temperature is exceeded. Hence temperature must be monitored within the applications for these reasons.

It is necessary to measure the temperature of chips accurately as it is operating. This is required because the reliability and speed of such CMOS circuits is affected by the temperature of the chips [4]. It is needed to measure a temperature sensitive electrical parameter in order to know the temperature of a chip as it operates. Hence, a temperature sensor should be designed in such a way that it uses that temperature sensitive parameter for measuring the chip temperature. Performance with high efficiency and low budget temperature sensors are in huge demands in the following utilization for the exceptional development of portable systems is becoming more than ever expected [5].

1. Control the heat dissipation on VLSI chips.
2. Compensate for the cross temperature sensitivity of other sensors in micro systems.
3. In automated consumer products like domestic appliances and cars.
4. In production plants that are automatic.

The most dominant aspect of temperature sensor is its power consumption apart from cost and performance. In order to fit the temperature sensor on a VLSI chip without manipulating the operating power of the chip, it is of utmost important that the sensor power is as minimum as possible [6]. Furthermore, also make such sensors feasible to be able to use in battery driven products to reduce errors due to self heating. It increases the power density significantly when multiple chips are integrated and fabricated as a one single chip. A "hotspot" is a generated localised area of high temperature resulting from huge switching activities in certain area of such a densely packed chip [7]. Unusual temperature gradients are caused by these hotspots across the chip which causes major threats to the robustness and reliability of the product. Thus, for the dependability of the system it is required that dynamic thermal management and on-chip thermal sensing is carried out properly. Consequently, it has become essential for the on-chip temperature sensors to be very energy efficient. This could be attained by the following two means:

1. If the temperature sensor idle state duration could be increased.
2. If a single temperature sensing operation energy consumption could be reduced.

A temperature sensor with high frequency would be good enough to meet these requirements. As this would result in faster completion of per temperature sensing operation and thus the sensor could have settled for more idle time in order to save energy consumption. Compact size is also important beside this higher conversion rate for both the smaller portable consumer products such as an ultrasonic probe or where multiple temperature sensors are needed to be placed for example a micro processor.

It has been always a seen phenomenon of rising temperature in current CMOS process technology than the previous one. This is because of the larger integration possible after every single time the CMOS process technology have scaled down in addition with the considerable amount of enhancement of the state-of-the-arts microprocessors [8]. Firstly, the consequences of the scenario with environment of such high temperature is the degraded functionality of the power management system due to the increased leakage of currents. Secondly, this temperature level is nearly associated with the life time of the product.So, it is a key job to monitor those thermal changes for the systems to be highly efficient. Also, it is not the correct way to measure the temperature of the chip by recording the temperature of the surface of the packaged chips over on-chip measurement since self-heating takes place. For that reason building of on-chip temperature sensors, for accurate thermal monitoring and management of the products, is embraced by huge numbers of commercial companies.

The advantages of the CMOS on-chip temperature sensors of low production cost and simpler interfacing with other electronic circuits made them superior over the traditionally temperature sensors which depends on off-chip components. Variations in the temperature effects the reliability and performance of a system and so it is essential to monitor these thermal changes using small sizes and low power temperature sensors [9]. These embedded temperature sensors are well known for their usage in the field of VLSI for illustrating excess heat dissipation on-chip over time due to higher and higher level of integration. There has big a boost in the evolution of such embedded temperature sensors after the exposure of RFID and wireless sensor network (WSN) applications. Power consumption is of supreme value rather than the required sensing accuracy and range for using in similar applications. These are the highlighted reasons which made this topic interesting and motivated for the work to be done passionately.

1.2 Goals and Objectives

Prior to this thesis, a variable gain amplifier with low power consumption and high bandwidth was designed for an ultrasonic probe used for medical imaging in the specialization project TFE4580 [1]. The schematic was drawn, simulated and verified in 90 nm CMOS technology using the leading software in analog industry called Virtuoso. A fully differential amplifier with source degeneration topology was used for varying amplification with better frequency response, stability, linearity and low noise power. All of the specifications provided were fulfilled by the implemented VGA and ensured accordingly using the simulation results.

Taking a step further from the specialization project, the goal and objective of the project has moved to designing and implementing a temperature sensor for the ultrasonic probe. The temperature sensor should be able to embed in the chips of the probes, hence should have low power consumption, cost and area. Again, the schematic is drawn, simulated and verified using the leading analog industry software namely Virtuoso. It was also mandatory to have minimum errors and maximum possible accuracy with better linearity, stability, sensitivity and lower noise. In addition, quite a temperature range should be considered for proper thermal monitoring of the ultrasonic probe with very low supply voltage and pulled current.

Schematic simulations were to be carried out for observing DC operating points and MOSFETs operating regions by the Virtuoso software. The output results and graphs from the simulations of the designed and implemented CMOS circuit for the temperature sensor were to be plotted and interpreted for verification, comparison and discussion. The corresponding errors of the designed temperature sensor were to be measured and noted for mentioning in the paper along with the sensitivity of the sensor for different process corner analysis. Monte Carlo simulations were to be executed for different run numbers with single number of point to know the resulting output and correlating errors, if this temperature sensors were to be fabricated in different chips. Noise analysis was also followed through to know about the noises caused in the temperature sensor circuit to avoid additional errors. The derived output besides errors graphs and relative tables with values and parameters data are provided in the result chapter.

1.3 Major Contributions

The following points are the highlighted major contributions that the designed and implemented on-chip temperature sensor exhibits.

- The CMOS temperature circuit has a mere power consumption of 131.2 nW for operating at the maximum temperature of 120 °C with power supply of only 600 mV and maximum drawn current of just 218.66 nA.
- A wide range of temperature from 0-120 °C is covered by the designed and implemented temperature sensor circuit.
- A sensitivity of +1 mv/ °C with error in the range of -3.3 to +7.6 °C is achieved through linear approximation.
- The temperature sensor is also suppose to occupy extremely small area as it is designed in 90nm CMOS process technology with widths and lengths of few hundreds of nano meters with few exception of high widths of some micro meters.

1.4 Report Structure

The rest of the report is organized in the following manner:
Chapter 2 - Background Theories : This chapter holds all the key theories and terms that are used in the report. It is important to get introduced with these information and knowledge for proper understanding of this report.
Chapter 3 - Methodology : The chosen solution is explained in this chapter with full detailing focusing on the approach and the reason of choice for selecting this solution suitable for the designated task.
Chapter 4 - Results and Analysis : All the results are presented in graphical and tabular form with appropriate interpretation of the outputs. The findings of the work are explained, evaluated and verified with genuine reasoning.
Chapter 5 - Discussion : Here, the outcomes of this implemented design work is discussed with different views and arguments for comparison with other similar works. Also, strengths and weaknesses of the project work is talk about in this chapter.
Chapter 6 - Conclusion and Future Works : This is the final chapter of the paper consisting of the summary of the entire work with highlighted parts of the work is revisited. In addition, the possible scope for improvement and extension of the work is illustrated.

Chapter 2

Background Theories

This chapter comprises of the theoretical background knowledge related to the design of a temperature sensor. It would not be possible to cover all the theories and also it would be unnecessary to include information that are not used in the implementation of the project. Hence, emphasis is put only to the theories that are more or less directly connected to the work. These are used as the building blocks for the project in the design process for the temperature sensor with proper reasoning for selection.

The objective of this chapter is to introduce the different types of temperature sensors that could be implemented along with different types of current mirrors for biasing the circuit in detailing. By doing so, the readers will have better grip and required understanding for assessing the implementation process report. The demonstrated topics here might be regarded as known to most of the people but it is always recommended to recollect those knowledge. Accurate references are provided were required for the sources of information used in the search of background theories with one being the specialization project done in the previous semester.

2.1 Temperature Sensor Circuit

A temperature sensing circuit could be constructed by a numerous number of ways. First of all, a temperature sensor could be realized in either of one of the 3 mentioned probable devices in CMOS technology as per the specifications requirement and those are the following [5]:

1. MOSFETs operating in weak inversion
2. Vertical bipolar transistors
3. Lateral bipolar transistors

Secondly, a circuit for temperature sensing classified into two more types

and they are as noted down [8]:

1. Voltage domain temperature sensor
2. Time domain temperature sensor

The voltage domain temperature sensors converts the measured temperature either into base-emitter voltage of a BJT or gate-source voltage of a MOSFET. Using an Analog-to-Digital converted (ADC), this voltage could be interpreted into a digital code. On the other hand, the time domain temperature sensor translates the evaluated temperature into a time delay proportional to this temperature change. And, a Time-to-Digital converter (TDC) is used to convert this delay to a digital code.

2.1.1 BJT-based Temperature Sensor

Temperature can be measured using a bipolar transistor substrate in most of the CMOS technology has been known for very long time. The difference in the base-emitter voltages of such substrate PNP transistors (diodes), when operating in different emitter current, could be used to measure temperature. This is because this difference in the voltage is proportional to the absolute temperature (PTAT) [10]. However, many external factors and non-idealities do effects this PTAT voltage but there are various ways for compensating them. In CMOS technology, two types of bipolar transistors are found namely (i) lateral bipolar transistors and (ii) substrate (vertical) bipolar transistor. The nature of the substrate bipolar transistor for behaving more ideally and being less sensitive to external pressure make them preferred [11]. Using the base-emitter voltage of such a substrate pnp transistor as a medium to compute temperature is the most forthright path to use it as a temperature sensor [12]. One important point to be noted is that every V_{BE} based temperature sensor is must to be calibrated using a reference temperature and voltage. The voltage $V_{BE}(T_r)$ is a very dominant problem here and thus the sensitivity is dependent on the process. Transistors operating at two different current densities whose base-emitter voltages difference (ΔV_{BE}) is used for tackling this problem of process dependency [13]. (ΔV_{BE}) is PTAT, with being independent of the absolute value of the collector currents and as well as no dependency on the process parameters, if the ratio of the collector currents is maintained to be a constant value. This attributes of (ΔV_{BE}) based temperature sensor makes it a great choice for worthy of use in integrated circuits.

2.1.2 Time-to-Digital Converter based Temperature Sensor

Another interesting method for measuring the temperature is to first generate a pulse which have a width proportional to the temperature using a temperature-

to-pulse generator. After that, the output pulse is supplied to the input of a cyclic time-to-digital converter (TDC) for converting to the equivalent digital output code for interpretation. A pulse responsive to the temperature could be produced using a straightforward circuit by taking advantage of gate delays. Then a delay line which is made up of even number of NOT gates, will cause a delay of a specific amount of time to the start signal. After that, this delayed signal can be XORed with itself to generate the necessary output pulse from the propagation delay of the delay line. Conventionally, an analog-to-digital converted (ADC) can also be used in place of a TDC. But, an ADC consumes much more power and occupies much more area then a TDC. A simple TDC is nothing again but delay line of an even number of serially connected NOT gates. The input signal revolve around the cyclic delay line after each reset. This circulated input signal is contracted by a certain amount of width per cycle before it is fully vanished. The co-relative digital output is then spawned by calculating the number of the input pulse rotations in the delay line by the counter.

2.1.3 MOSFET-based Temperature Sensor

MOSFET's could be used as constituents for sensing of surrounding temperature when they are operating in sub-threshold region. Their gate-source voltage is taken into consideration for perceiving the absolute temperature. Utilizing an ADC, this voltage might be fed and converted to corresponding digital output. Very lower power consumption is attainable because of the operation of the MOSFETs in the sub-threshold region where the gate-source voltage is lesser than the threshold voltage.

A proportional to absolute temperature (PTAT) current generator circuitry is displayed in the figure 2.1. A switched capacitor is included in replacement for a traditional resistor and the circuit is build upon a β multiplier self biasing sub-circuit. When this circuit set up is run in the strong inversion region, it acts as a constant Gm biasing circuitry. On the other hand, the same circuit behaves as a PTAT current generator, when it is operated in the sub-threshold region. A capacitor C_{S2} and two switches sw3 and sw4 are used to build the switched capacitor sub-circuit, which is directed with an external reference clock with frequency f_{REF}. The equivalent resistance R_{SC}, between the source node of M_2 and the ground, is evaluated to $(C_{S2}f_{REF})^{-1}$. Hence, this equivalent resistance R_{SC} can be manipulated by changing the external reference clock with different frequency f_{REF}. Moreover, few hundreds of nano ampere or less current is drawn by the MOSFETs as they are biased in the sub-threshold region, making it an ultra low current operated circuit.

The drain current I_D of the MOSFET biased in a sub-threshold region

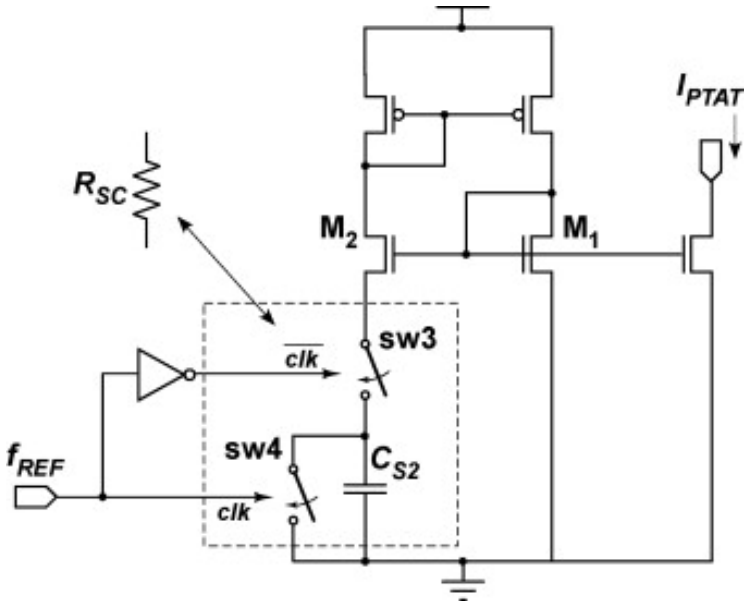

Figure 2.1: A PTAT current generator. [14]

exhibits an exponential function in terms of gate-source and drain source voltages. The equation of this drain current I_D is given by:

$$I_D = KI_0 exp(\frac{V_{GS} - V_{TH}}{\eta V_T})(1 - exp(\frac{-V_{DS}}{V_T})) \tag{2.1}$$

$$I_0 = \mu C_{OX}(\eta - 1)V_T^2 \tag{2.2}$$

where,

- K is the aspect ratio (W/L)
- μ is the carriers mobility
- C_{OX} is the gate-oxide capacitance
- V_T (K_BT/q) is the thermal voltage
- k_B is the Boltzmann's constant
- T is the absolute temperature in °K
- V_{TH} is the threshold voltage
- η is the sub-threshold slope factor [15]
- q is the electron charge

The equation for the drain current I_D can be simplified down to the following when drain-source voltage V_{DS} is greater than 0.1 V:

$$I_D = KI_0 exp(\frac{V_{GS} - V_{TH}}{\eta V_T}) \tag{2.3}$$

The gate-source voltage V_{GS1} of the MOSFET M_1 can be written as the sum of the gate-source voltage V_{GS2} of the MOSFET M_2 and voltage drops across the switched capacitor resistor R_{SC}, that is:

$$V_{GS1} = V_{GS2} + I_{PTAT}R_{SC} \tag{2.4}$$

Equal amount of current is driven through the MOSFETs M_1 and M_2, therefore the expression formulated for output current I_{PTAT} of the PTAT current generator is as follows:

$$I_{PTAT} = \frac{\eta V_T ln(K2/K1)}{R_{SC}} = f_{REF}C_{S2}\frac{\eta k_B T}{q}ln(\frac{K2}{K1}) \tag{2.5}$$

Here, the output I_{PTAT} current is proportional to the absolute temperature because both of the C_{S2} capacitance and f_{REF} frequency of the external reference clock are constants, hence independent of the temperature.

2.2 Current Mirrors

A current mirror is a circuit which can be used to copy current from one branch of active transistor to one or more branches of active transistor(s) by controlling and manipulating the current through one of them. Their basic usage incorporates supplying bias current for ensuring that the transistors are operating in the desired region and also can be employed as an active load in an electronic circuit. Regardless of the output load, the output current can be kept constant with the help of such circuitry.

2.2.1 CMOS Current Mirror

This portion of the background information is taken from the previous specialization project [1] with no new material found on this. A CMOS current mirror is a two-port circuit which takes an input current I_{in} and generates an equivalent output current $I_{out} = I_{in}$ ideally when both the transistors are of same sizes and operating in the active region as shown in the figure 2.2. The input resistance of an ideal current source is zero and the output resistance is infinite. Thus the current mirror is able to mimic the input current regardless of the source and load impedances connected because it has low input resistance of $1/g_{m1}$ and high output resistance of r_{ds_2}.

2.2.2 Cascode Current Mirror

A cascode current mirror is illustrated in the figure 2.3 and looking into the drain of Q2 it can be simply examined that r_{ds2} is the output impedance. It

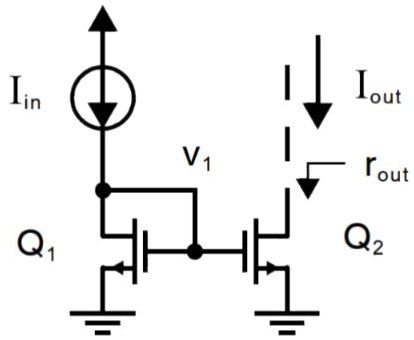

Figure 2.2: A CMOS current mirror. [16]

is same as that of a CMOS traditional current mirror. Henceforth, thinking of Q4 as a current source with a source-degeneration resistor value of r_{ds2}, the output impedance can be evaluated easily. The output impedance of a CMOS current mirror gets multiplied by the gain of the cascode device $g_m R_{ds}$ due to its addition. It reduces the available output voltage swing as a part of this is used to keep the cascoded transistors in the active region.

2.2.3 Full Wilson Current Mirror

The circuit for the full Wilson current mirror is shown in the figure 2.4. From the figure it can be concluded that for a constant I_{in}, V_{DS} of the MOSFETs M1, M2 and M4 are held at a fixed value. This results in the advantages of increased output impedance and stabilizes the output current I_{out} further more, that is, its accuracy is enhanced. The output impedance can be denoted as:

$$R_O \approx g_m r_{O3} r_{O2} \tag{2.6}$$

It can be used where very high currents are required as it consists of 4 transistors. It provides very low resistance at the input side. Also, it does not require any other external biasing.

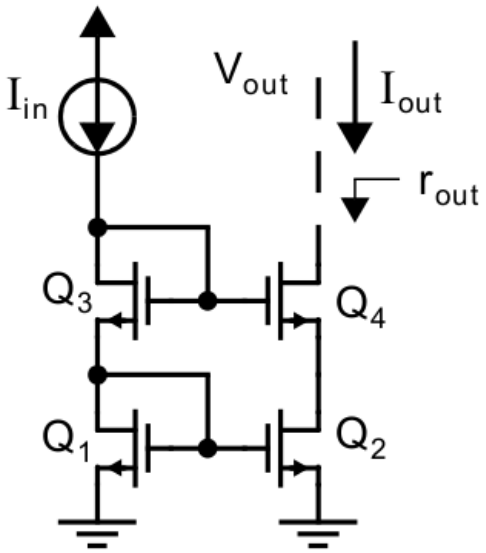

Figure 2.3: Cascoded current mirror. [16]

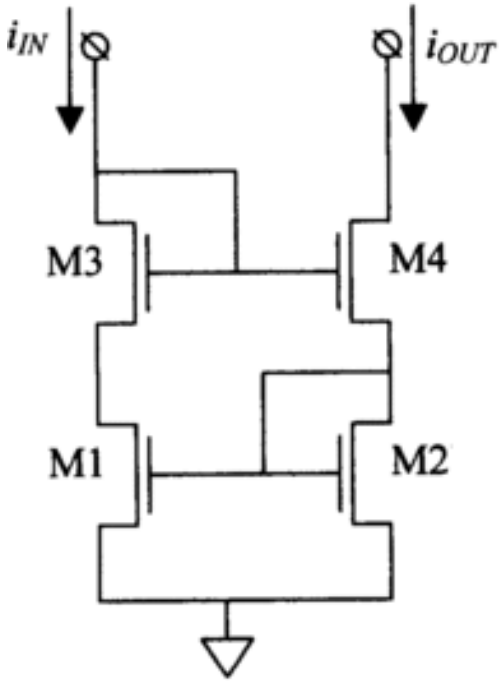

Figure 2.4: Full Wilson current mirror.

Chapter 3

Methodology

The third chapter is basically about the methodological approach adopted for the accomplishment of the project. The reasons for the choices of the method and design are explained here in detailing that is appropriate for the plan of the temperature sensor for an ultrasonic probe. Even the strengths and weaknesses along with the proper means of collecting and interpreting the collected data is mentioned here.

In general, there are three performance metrics for the evaluation of an analog circuit which are showed below with a performance metric triangle in the figure 3.1.

1. Power
2. Accuracy
3. Speed

In real life it is not possible to design an analog circuit that will have the minimum power consumption in addition with maximum speed and accuracy.

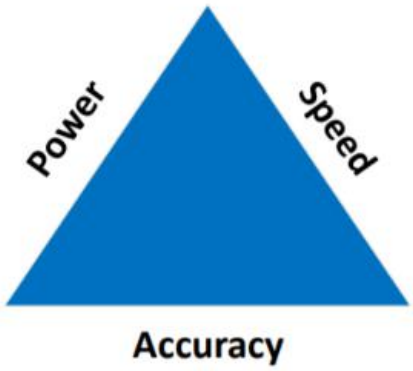

Figure 3.1: A performance metric triangle.

There have to be made a trade off between each of these elements in the performance metric triangle. The choices are made by the analog designers in accordance with the requirement of the given specifications. Though it could be though of as a problem in the designing methodology, but keeping these things in mind and crossing over these hurdles, the following temperature sensor design is achieved for an ultrasonic probe.

3.1 Design Architecture

First of all, 90 nm CMOS process technology is for the design and implementation of the designed temperature sensor. It's lower power consumption ability along with low cost makes it a very powerful competitor in comparison with Bi-polar or Bi-CMOS process technologies which are more power hungry and costlier [17]. Hence, it is the best choice for building our designed temperature sensor.

Secondly, as mentioned earlier a temperature sensor can be realized in two ways which are (i) voltage domain and (ii) time domain. The time domain temperature sensor occupies larger areas and consumes more power at the required sampling rate [18]. This is the reason, voltage domain temperature sensor approach is applied in the designing and implementation of the required temperature sensor.Also, it is found from many papers that recently this type of temperature sensor have achieved higher accuracy and resolution.

Again, a voltage domain temperature sensor could be implemented by using either BJT transistors or MOSFET transistors. Bi-polar type of sensors have been found to have very good accuracy in general, but comes with the cost increased circuit complexity, power consumption and chip area [18]. But, as our target device is a portable ultrasonic probe, power consumption and area are of more concern than accuracy. Thus, we opt for the MOSFET based temperature sensor as the basic building block, which is explained about in the chapter 2 of theoretical background.

The designed architecture which is demonstrated in the figure 3.2 is based on the work of a published paper [18]. It comprises of a current source sub-circuit, which is an improved version of Wilson current mirror. It is used because of its advantages of more stabilize and accurate current generation with very low input resistance and very high output resistance, over the traditional or cascoded current mirror, as have been mentioned earlier in the chapter 2. The MOSFETs (M1-M5) employs such a current mirror which is self biased and produces current independent of the loads and voltage sources. The current mirror is biased and operated in the sub-threshold region. The produced current is then copied by the MOSFETs (M12-M14) and supplied to the temperature variable sub-circuit.

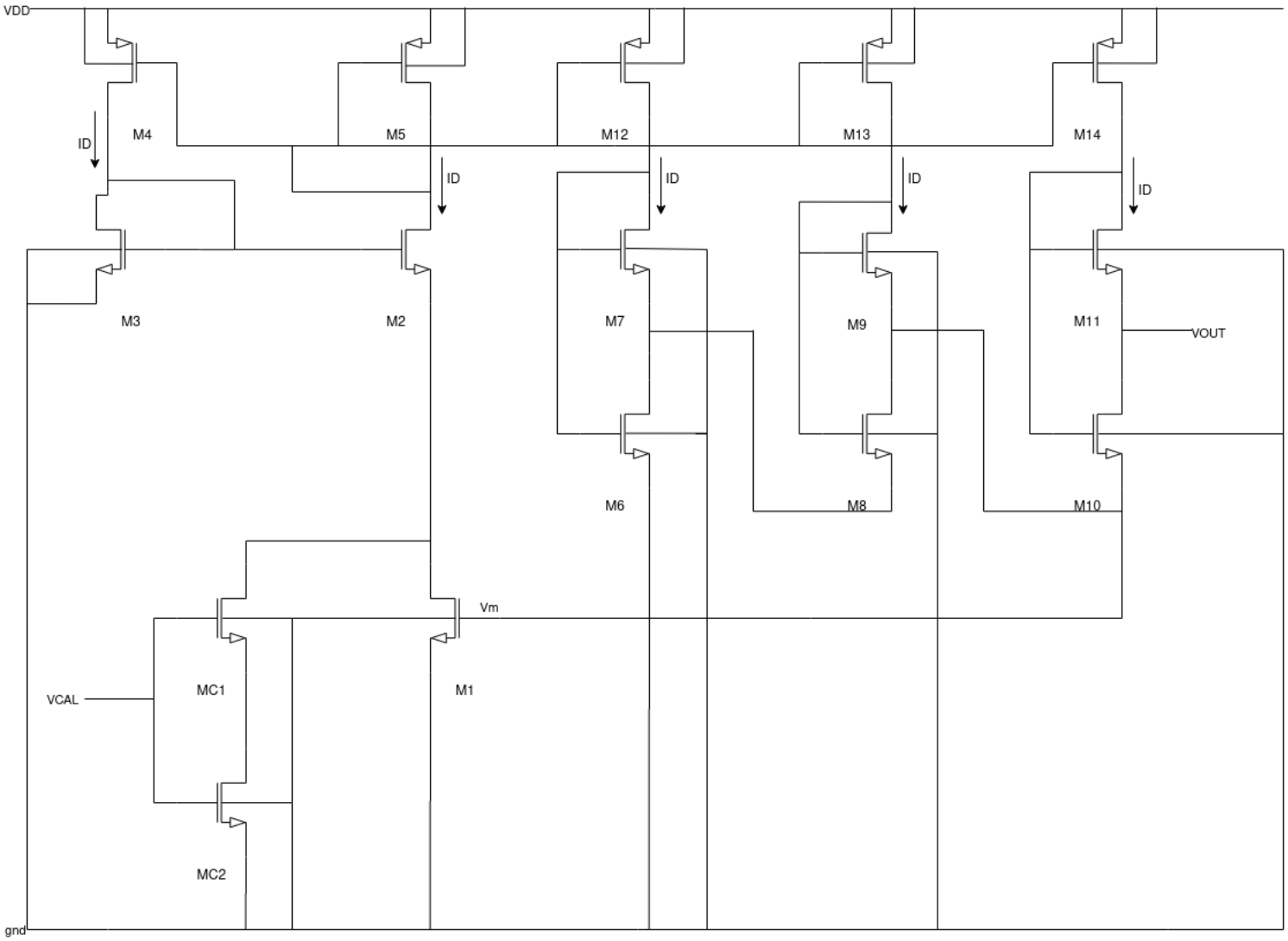

Figure 3.2: The Designed Temperature Sensor Circuit.

Three pairs of serially connected MOSFETs (M6-M11) is used to configure the temperature variable sub-circuit as can be seen from the figure 3.2. The root of this configuration came from the MOSFET-based temperature sensor discussed in the chapter 2. It was said in the chapter that drain current and gate-source voltage of a MOSFET running in sub-threshold region exhibits an exponential function. This is similar to the relationship of collector correct I_C and base-emitter voltage V_{BE} of a BJT transistor as described in the second chapter of this report. The deduction of the summed gate-source voltages of M7, M9 and M11 from that of M6, M8 and M10 gives the overall output voltage of the designed circuit, which is found to express a linear relationship with the absolute temperature. The configuration of the operating MOSFET's in the sub-threshold region makes it possible to achieve very low power consumption.

At the end, the MOSFET's MC1 and MC2 build up the one point calibration sub-circuit. This is used for calibrating the temperature sensor by measuring the on-chip temperature at a reference point after packaging.

3.2 Designed Circuit Description

All of the equations in this section of the chapter are from the paper [24] on which this designed temperature circuit is based on. It has been mentioned several times that the drain current I_D of a MOSFET configured in a sub-threshold region represents an exponential behaviour with regard to the gate-source V_{GS} and drain-source voltages V_{DS}. The expression is as follows:

$$I_D = KI_0 exp(\frac{V_{GS} - V_{TH}}{\eta V_T})(1 - exp(\frac{-V_{DS}}{V_T})) \tag{3.1}$$

Here,

$$I_0 = \mu C_{OX}(\eta - 1)V_T^2 \tag{3.2}$$

- K is the aspect ratio (W/L)
- μ is the carriers mobility
- C_{OX} is the gate-oxide capacitance
- V_T is the thermal voltage
- V_{TH} is the threshold voltage
- η is the sub-threshold slope factor [15]

The drain current I_D for a MOSFET has no dependency on the drain-source voltage V_{DS} when it is above 0.1 V and thus the equation 3.1 is reduced into the following expression:

$$I_D = KI_0 exp(\frac{V_{GS} - V_{TH}}{\eta V_T}) \tag{3.3}$$

The summation of the gate-source voltage of M2 and drain-source voltage of M1 is equivalent to the gate-source voltage of M3 of the Wilson current source sub-circuit. Therefore:

$$V_{GS3} = V_{DS1} + V_{GS2} \tag{3.4}$$

Or, it could be also written as:

$$V_{DS1} = V_{GS3} + V_{GS2} \tag{3.5}$$

This equation 3.5 could be further broken down into the following expression by using the equation 3.3:

$$V_{DS1} = \eta V_T ln(\frac{K2}{K3}) \tag{3.6}$$

Next step is to look into the output conductance of the MOSFET M1 operated in sub-threshold region and is given by the following equation:

$$G_{DS1} = \frac{\delta I_{DS1}}{\delta V_{DS1}} \tag{3.7}$$

Substituting equation 3.1 and 3.6 into the above equation 3.7, results in the following expression for the output conductance of M1:

$$G_{DS1} = \frac{K_1 I_O}{V_T} exp(\frac{V_m - V_{TH1}}{\eta V_T} - \frac{V_{DS1}}{V_T}) \tag{3.8}$$

The current through all the branches are same and hence the equation for current through M1 is the following:

$$I_D = V_{DS1} \times G_{DS1} \tag{3.9}$$

Then by substituting the equations 3.6 and 3.8 into the above equation 3.9, the below expression is derived:

$$I_D = \eta K_1 I_O (\frac{K3}{K2})^{\eta} ln(\frac{K2}{K3}) exp(\frac{V_m - V_{TH1}}{\eta V_T}) \tag{3.10}$$

From a published paper [19], it is founded that there is a linear relationship between threshold voltage of a MOSFET and the absolute temperature. It is expressed by the equation below:

$$V_{TH} = V_{THO} - 2V_T ln(\frac{n}{n_i}) \tag{3.11}$$

And,

$$V_T = \frac{K_B T}{q} \tag{3.12}$$

Where,

- k_B is the Boltzmann's constant
- T is the absolute temperature in °K
- q is the electron charge
- n is the carrier concentration
- n_i is the intrinsic carrier concentration

It can be observed from the equation 3.10 that the current I_D is increased by temperature, because the voltage V_m - V_{TH1} is less than 0, as the operating point of M1 is sub-threshold. So, it can be said that the maximum current is drawn at the highest temperature which could be restricted using the dimension of the MOSFETs. Therefore, a trade off have to be made between power and linearity for fixing the maximum available current. In order to achieve a suitable point in such a trade off, several simulations were carried out.

The generated current I_D is nearly constant and have no voltage source dependency in the wide range of voltage sources because of the self biasing improved Wilson current mirror sub-circuit. This current is supplied to the temperature variable sub-circuit to produce the output voltage which has linear relationship with the temperature.

The MOSFETs M6-M11 are also operating in the sub-threshold region in the temperature variable sub-circuit. Hence, equation 3.3 could be used for the relationship between gate-source voltages and currents through those MOSFETs. The value of currents flowing through the MOSFETs M7, M9, M10 and M11 is I_D, whereas current though M8 is $2I_D$ and M6 is $3I_D$ accordingly to the figure 3.2. Summation of the gate-source voltages along M6-M11 would result in the output voltage of the temperature sensor and the expression for this is given below:

$$V_{OUT} = V_{GS6} - V_{GS7} + V_{GS8} - V_{GS9} + V_{GS10} - V_{GS11} \tag{3.13}$$

The usage of the equation 3.3, results in the expansion of the above equation as follows:

$$V_{OUT} = \eta V_T ln(\frac{I_{D6}I_{D8}I_{D10}K_7K_9K_{11}}{I_{D7}I_{D9}I_{D11}K_6K_8K_{10}}) + \Delta V_{TH} \tag{3.14}$$

where ΔV_{TH} is the equivalent threshold voltage of all the MOSFETS through M6-M11:

$$\Delta V_{TH} = V_{TH6} - V_{TH7} + V_{TH8} - V_{TH9} + V_{TH10} - V_{TH11} \tag{3.15}$$

The expression above is more simplified by substituting the current values and the resulting equation becomes:

$$V_{OUT} = \eta V_T ln(\frac{6K_7K_9K_{11}}{K_6K_8K_{10}}) + \Delta V_{TH} \tag{3.16}$$

Finally, the required output voltage is obtained by merging the equation 3.16 with 3.12 and thus the expression is:

$$V_{OUT} = \eta \frac{K_B T}{q} ln(\frac{6K_7K_9K_{11}}{K_6K_8K_{10}}) + \Delta V_{TH} \tag{3.17}$$

This expression 3.17 could be generalized as an equation for a straight line as follows:

$$V_{OUT} = mT + c \tag{3.18}$$

with the gradient m being:

$$m = \eta \frac{K_B}{q} ln(\frac{6K_7K_9K_{11}}{K_6K_8K_{10}}) \tag{3.19}$$

and the y-intercept c of:

$$c = \Delta V_{TH} \tag{3.20}$$

The equation 3.18 illustrates a linear behaviour of output voltage with respect to the absolute temperature. The variable in the equation is, T as the absolute temperature in Kelvin scale, with m and c being constant values which are not dependant on the temperature. The aspect ratio K6-K11 of the MOSFETs M6-M11 respectively and ratio of currents could be used for controlling the gradient m of the straight line. A precise co-efficient of temperature variable could be anticipated if the lengths of the MOSFETs M6-M11 are kept very larger than the minimum gate length of the technology. By doing so, we can minimize the vulnerability of the transistors to the process and geometric variations as well as the influence of the random doping fluctuations on the threshold voltages. MC1, MC2 and VCAL is used to adjust the y-intercept c, which has a dependency on the current I_D.

It was very difficult to find the correct sizes, that is length, width and multiplier, for each of the transistor used in the designed temperature sensor circuit. A huge number of simulations were done by changing the lengths, widths and multiplier value with numerous iterations to find the correct combination that well suited the requirements. Though it was hectic work, but in analog engineering there is no way around to this. Initially, the sizes of transistors M6-M11 were altered several times and simulated to find the combination that makes the gradient as close to one at the reference temperature of 65 °C. Then, manipulating the sizes of transistors M1-M5 to, to vary the current which fixes the y-intercept, as well as the drawn current is dependent on them. Finding the suitable combination of sizes for M1-M5 was also a difficult task and again various large number of simulated iterations were carried out.

Chapter 4

Results and Analysis

This is the main chapter of the report for portraying the methodologies used for testing the designed temperature sensor circuit and obtaining the corresponding results are described. The post-layout simulations resulting data and graphs are then analysed and verified by disclosing, explaining and assessing the discoveries of the project work in details. The leading analog industry software named Virtuoso is used for the purpose.

4.1 Testing Methodology

First of all, the schematic of the designed circuit for the temperature sensor is drawn with the help of the Virtuoso software schematic L editor. Then, it is created into a block sing the software in order to be able to be used as a testbench for the verification process and correlated results generation. This created testbench is shown in the figure 4.1. The rectangular block denotes the entire circuit designed for the temperature sensor as a black box to be tested and verified. The required voltages VCAL and VDD are supplied using the traditional DC sources and the output is observed across the capacitive load CL. The other voltage source V in series with resistor R is used for the generation of the ideal straight line in comparison with the actual output.

4.2 Analysis Methodology

There are several types of analyses provided by the software Virtuoso, which can be deployed on the testbench for the generation of results and verification purposes. The simulator is called ADE L which is capable of performing such analyses over the testbench enabling us to look at the output along with various other parameters presents in the circuit that is put under test. Our favoured

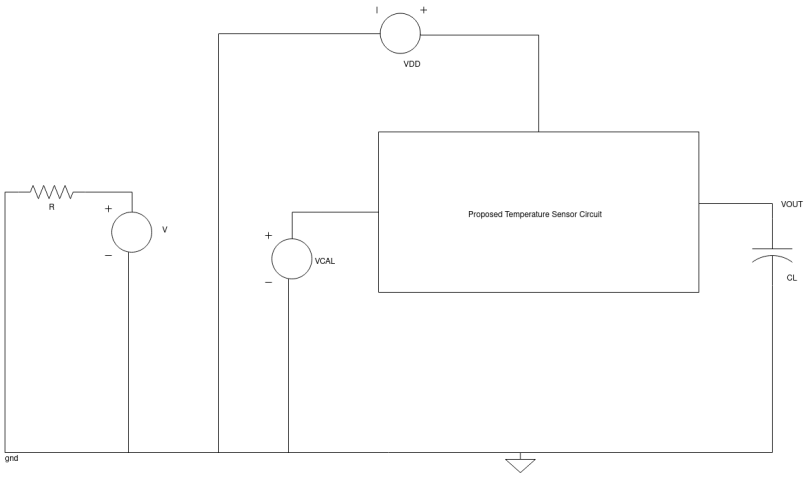

Figure 4.1: The created testbench.

type of analyses is the DC analysis because we are interested to see the output DC voltage as a function of temperature. It can be divided into further two sub-groups namely, (i) Numerical and (ii) Graphical analysis. Both of them are carried out and the outcome is discussed in the following sub-sections.

4.2.1 Numerical Analysis

This is the type of DC analysis which is numerical in nature. Such an analysis is capable of reflecting all the major parameters of each of the transistors used in the testbench such as width, length, transconductance, β, etc, in addition with each node current and voltages. These valuable information could be used to verify the region of operation of each of the MOSFETs from M1-M14. Furthermore, the power dissipation can be calculated from the node voltage and currents as illuminated by the simulator. For this purpose, there is a option in the ADE L, called annotate DC operating points, which shows all of the above mentioned attributes on the circuit schematic. The designed circuit is simulated at the reference temperature of 60 °C (taken as the mid-point between the range of 0-120 °C) with VDD of 600 mV and VCAL of 125 mV. The obtained DC operating points of the designed temperature sensor for an ultrasonic probe is represented in the table 4.1.

4.2.2 Graphical Analysis

This is the type of DC analysis where the output voltage graph is plotted by sweeping the temperature from 0-120 °which is shown in the figure 4.2.

Then, the derivative of this output graph was taken and plotted using the

Transistor	I_D (nA)	V_{DS} (mV)	V_{GS} (mV)	W (nm)	L(nm)	Multiplier	Operating Region	Function
M1	17.39	37.03	157.56	180	2400	1	Sub-threshold	Current Mirror
M2	21.64	441.74	14.64	360	360	10	Sub-threshold	Current Mirror
M3	22.35	51.71	51.71	360	360	4	Sub-threshold	Current Mirror
M4	-22.33	-548.29	-121.18	360	1200	1	Sub-threshold	Current Mirror
M5	-21.63	-121.18	-121.18	360	1200	1	Sub-threshold	Current Mirror
M6	66.47	82.09	153.39	120	360	1	Sub-threshold	Temperature
M7	22.23	71.29	71.29	360	360	3	Sub-threshold	Temperature
M8	44.24	75.46	147.25	120	360	1	Sub-threshold	Temperature
M9	22.16	71.78	71.78	360	360	4	Sub-threshold	Temperature
M10	22.09	83.37	128.16	120	360	1	Sub-threshold	Temperature
M11	22.09	44.79	44.79	360	360	14	Sub-threshold	Temperature
M12	-22.23	-446.61	-121.18	360	1200	1	Sub-threshold	Current Mirror
M13	-22.15	-370.66	-121.18	360	1200	1	Sub-threshold	Current Mirror
M14	-22.09	-314.28	-121.18	360	1200	1	Sub-threshold	Current Mirror
MC1	4.24	22.17	110.09	120	2400	1	Sub-threshold	Calibration
MC2	4.24	14.91	125	120	2400	1	Sub-threshold	Calibration

Table 4.1: DC operating points of the MOSFETs

calculator available in the ADE L simulator is given in the figure 4.3. The gradient at the reference temperature of 60 °C is marked, which is later used to extract the ideal straight line equation for our designed temperature sensor. According to the equation 3.19, the gradient is proportional to the aspect ratio of the MOSFETs from M6-M11, which could be manipulated to get the required gradient. The aim was to target for gradient as close to 1, so that we will be able to extract a straight line where 1 mV corresponds to 1 C, that is the sensitivity of the designed temperature sensor (1 mV/°C). Several attempts were made by simulating the circuit with different combinations of the aspect ratio for the MOSFETs M6-M11, until the appropriate value was extracted.

Finally, the ideal straight line plotted by extracting the equation from the gradient and the point where it meet the actual graph at the reference point of 60 °C. Using the gradient from the figure 4.3 and the point in the figure 4.1 respectively, the following ideal best fit line equation was derived with temperature T in °C scale and represented in the figure 4.4:

$$V_{OUT} = 180.916mV + 1.0003T^{\circ}C \tag{4.1}$$

This ideal equation can then be more approximated to get the equation for the approximated ideal line as:

$$V_{OUT} \approx 181mV + T^{\circ}C \tag{4.2}$$

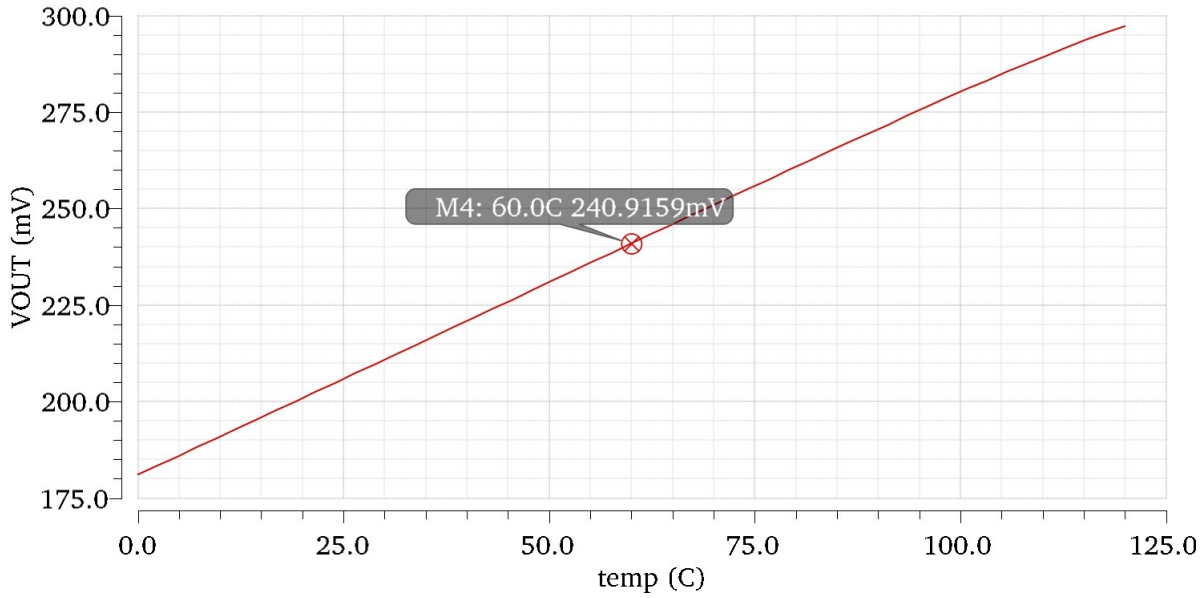

Figure 4.2: The actual output graph of the designed temperature sensor.

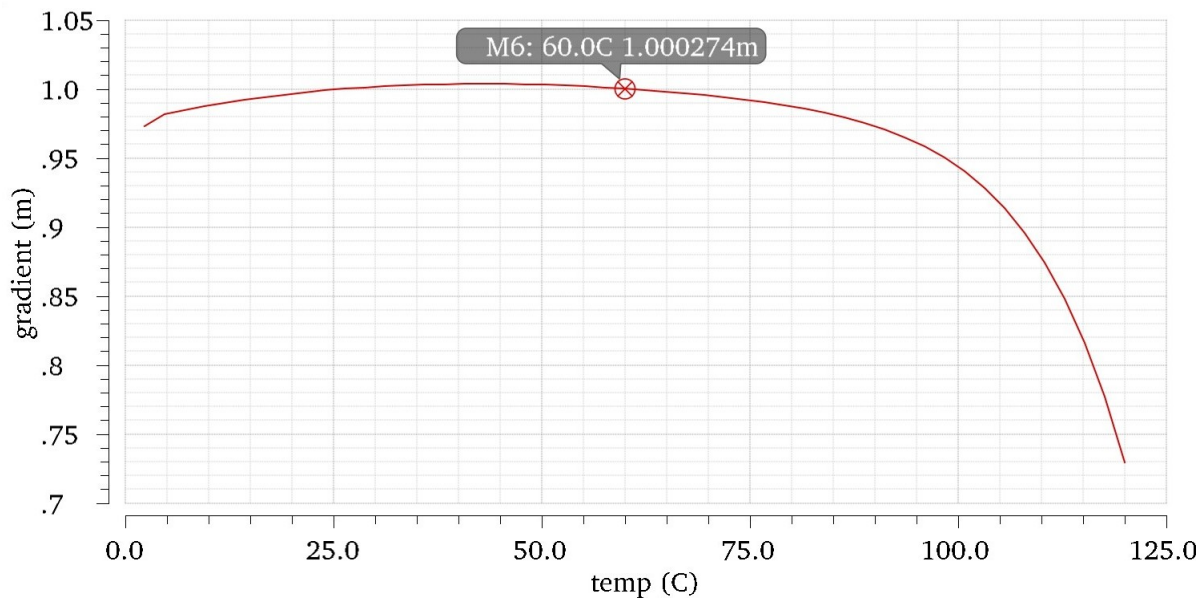

Figure 4.3: The derivative graph for the output of the designed temperature sensor.

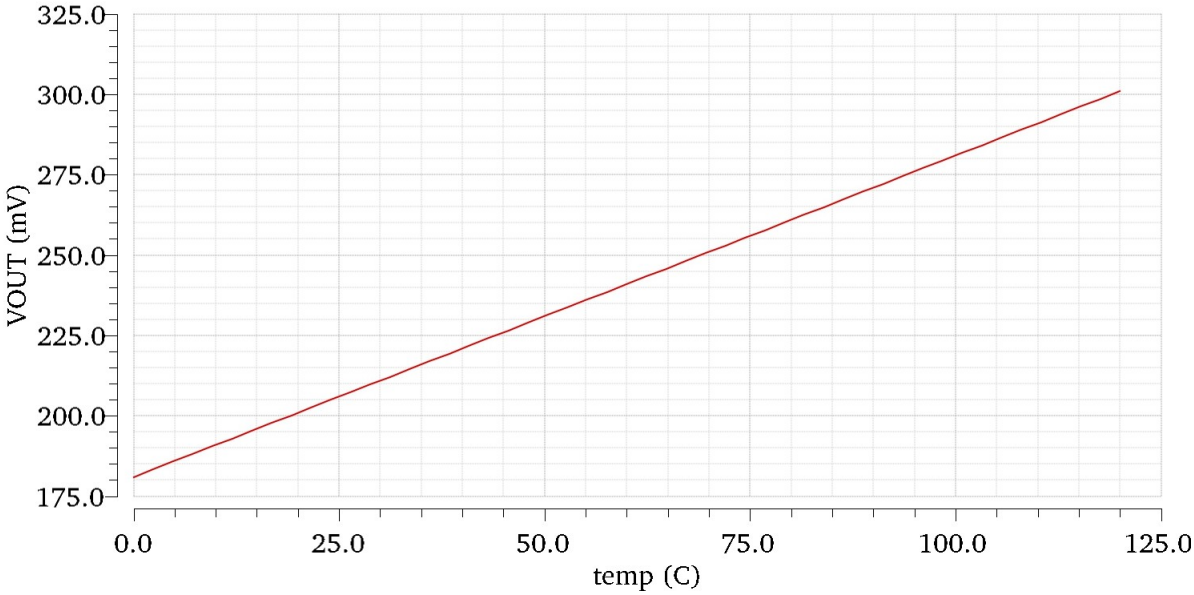

Figure 4.4: The graph of the extracted ideal line.

Next, the error between the actual output and ideal line which is the inaccuracy of the designed temperature sensor was calculated. It was produced by subtracting the actual graph from the ideal one once again with the help of the calculator in the ADE L of the Virtuoso software. All the simulation till now were run on the TT process corner, that is for a typical NMOS and a typical PMOS. The error graph is displayed in the figure 4.5 with error of -0.2 to +3.7 °C.

Now, the entire algorithm was run over again twice for the SS and FF corners corresponding to a slow NMOS and a slow PMOS and a fast NMOS and a fast PMOS respectively. The correlated actual output graphs are accumulated to present in the figures 4.6 for all the three process corners of TT, SS and FF to observe the effect on the process corners on the output voltage with respective to the absolute temperature in °C scale. It can be concluded from the graphs in the figure 4.6 that the output remains similar in all the cases with equal gradient but different y-intercepts. For the SS corner, the y-intercept went below than the TT corner, whereas the y-intercept for the FF corner went up by the same amount.

The corresponding ideal lines are plotted in the figure 4.7 for all the three process corners. The similar fashion is expected to be observed like those of the actual output lines with gradients almost equal to 1 and y-intercept being moved down in the case of SS process corner simulation while moved up in the case of FF corner respectively.

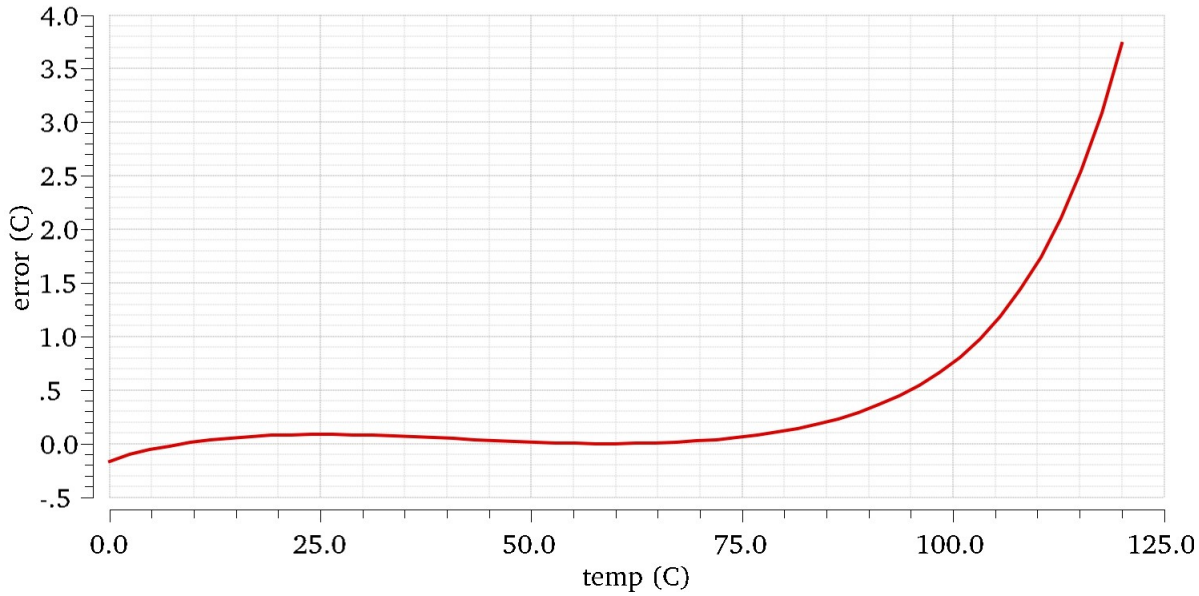

Figure 4.5: The error graph of the designed temperature sensor.

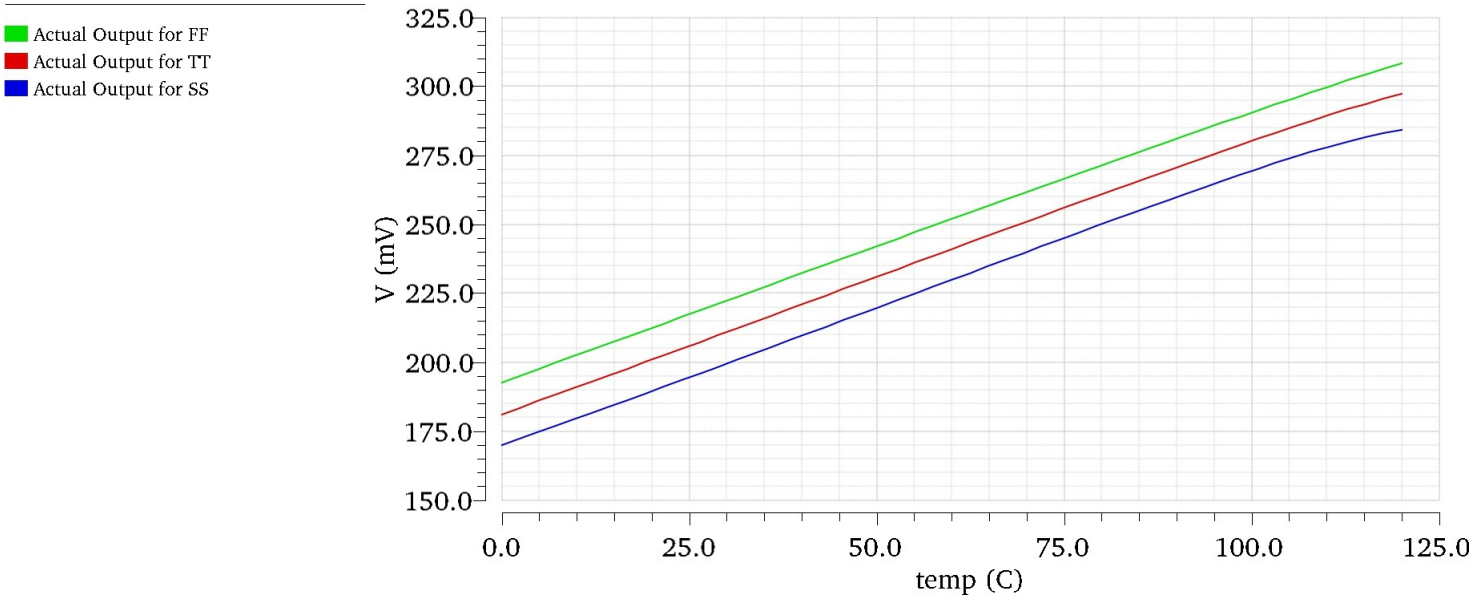

Figure 4.6: The actual output graph of the designed temperature sensor for TT, SS and FF.

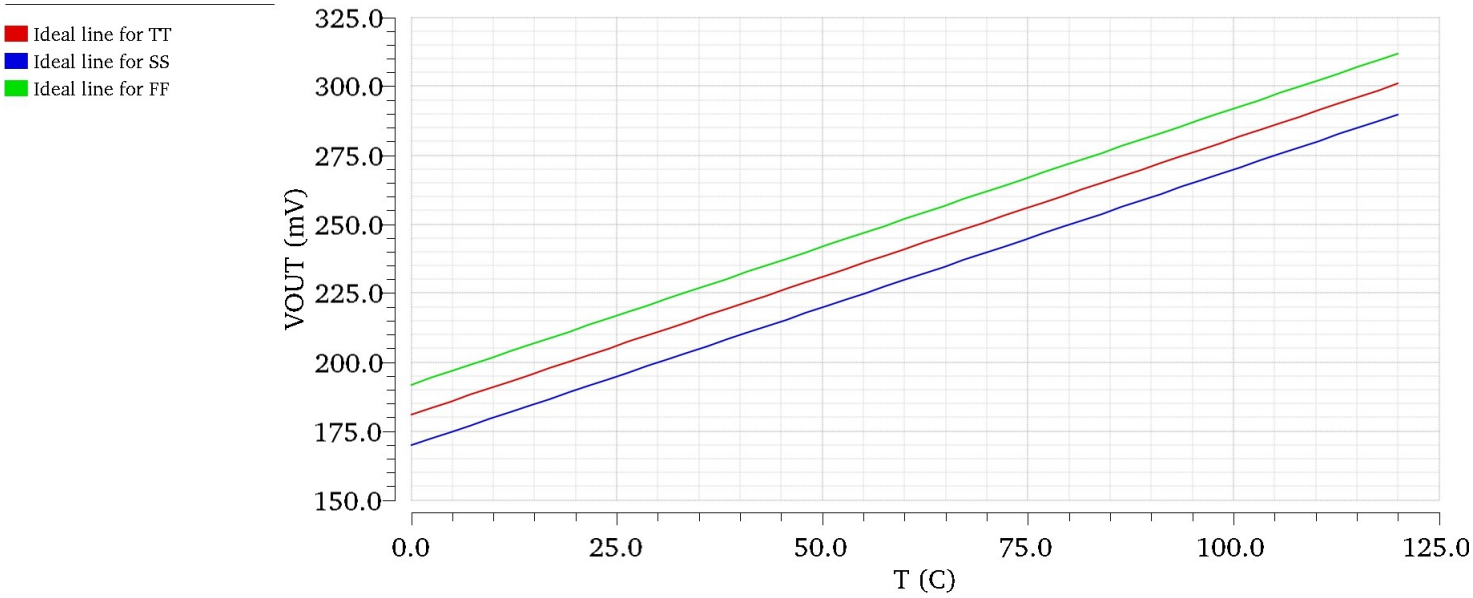

Figure 4.7: The ideal line graph of the designed temperature sensor for TT, SS and FF.

The exact equation for the ideal lines in both the scenario is given by the equations 4.3 and 4.4.

For the FF corner, the equation for the ideal line is:

$$V_{OUT} = 191.816mV + 0.980T^{\circ}C \tag{4.3}$$

And, for the SS corner, the equation for the ideal line is given by:

$$V_{OUT} = 169.775mV + 1.014T^{\circ}C \tag{4.4}$$

Now, the corresponding errors of the designed temperature sensor for the different process corners are observed. It is very important to have a look at them as they denote the inaccuracy of the implemented temperature sensor on different process corners. The graph is included in the figure 4.8 for comparison and deciding which process corner should be used for the fabrication of the sensor, and thus respective ideal line equation could be used for measurement of the surrounding temperature.

It can be observed from the graph that inaccuracy range in SS has changed to -0.2 to +5.6 °C whereas that of FF has moved to -0.8 to +3.6 °C. When compared with the TT process corner, the upper range of error in SS is seen to be quite high and the lower range remains almost the same. On the other hand, error upper range is 0.1 °C less in case of FF but the lower range has moved down by 0.6 °C which is not a big issue when compared to changes in SS

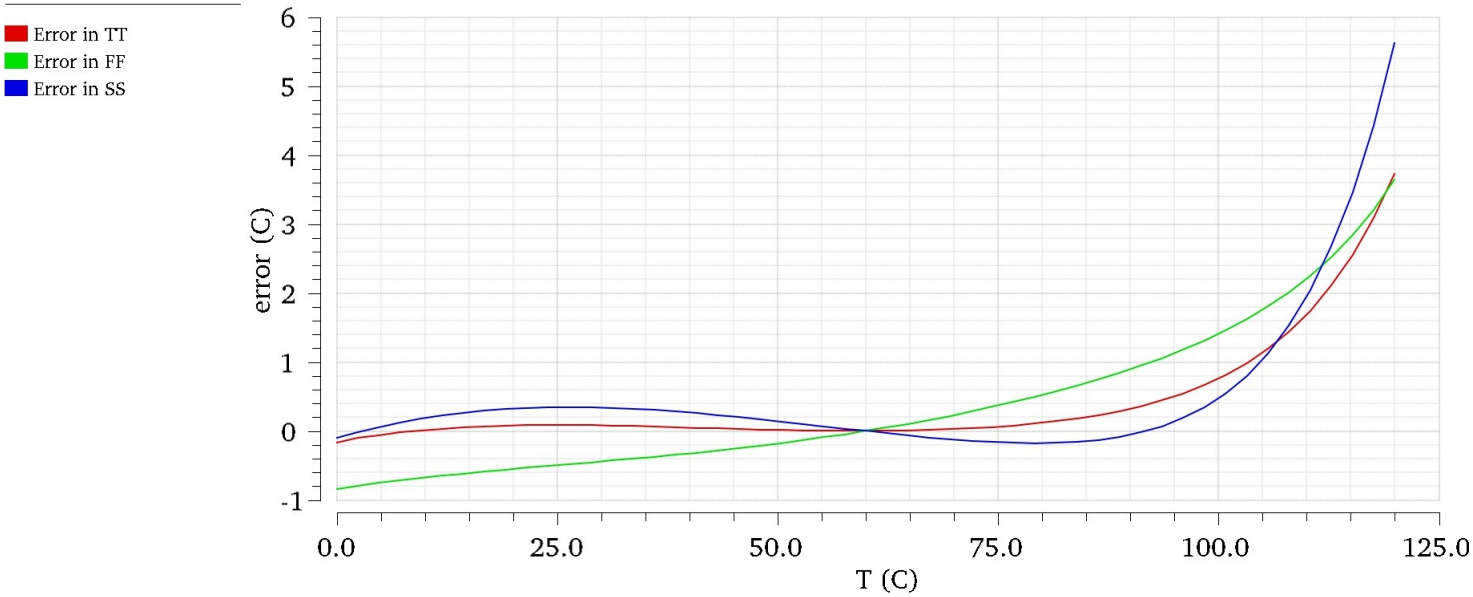

Figure 4.8: The corresponding errors of the designed temperature sensor for TT, SS and FF.

corner. After all these comparisons and discussions, it seems that FF process corner is more favourite than SS because of its huge upper range difference which adds almost 2 °C inaccuracy in the measurement of the surrounding temperature.

When the temperature range is reduced to 0-110 °C, the errors for TT, SS and FF are impressively lesser than the previous range. The error range is cut down to as much as -0.8 to +2.2 °C for the FF process corner. The inaccuracy range for the TT and SS processes are -0.2 to +1.7 °C and -0.2 to +1.9 °C, respectively as shown in the figure 4.9.

Figure 4.10 shows the errors in the different process corners for further reduced temperature range of 0-100 °C. The error in the temperature is further decreased as far down as to -0.2 to +0.5 °C for the SS corner. The inaccuracy drop for the TT and FF process corners are -0.2 to + 0.8 °C and -0.8 to + 1.4 °C, respectively.

4.2.3 Monte Carlo Simulation

Monte Carlo simulations were carried out with the help of ADE XL simulator in the software Virtuoso. It was set up with 1 number of point to look for the mismatch, with different run number/chip number by disabling the nominal simulation run. This was done to look for the errors over the temperature range from 0-120 °C, that might result when the chips are fabricated in the

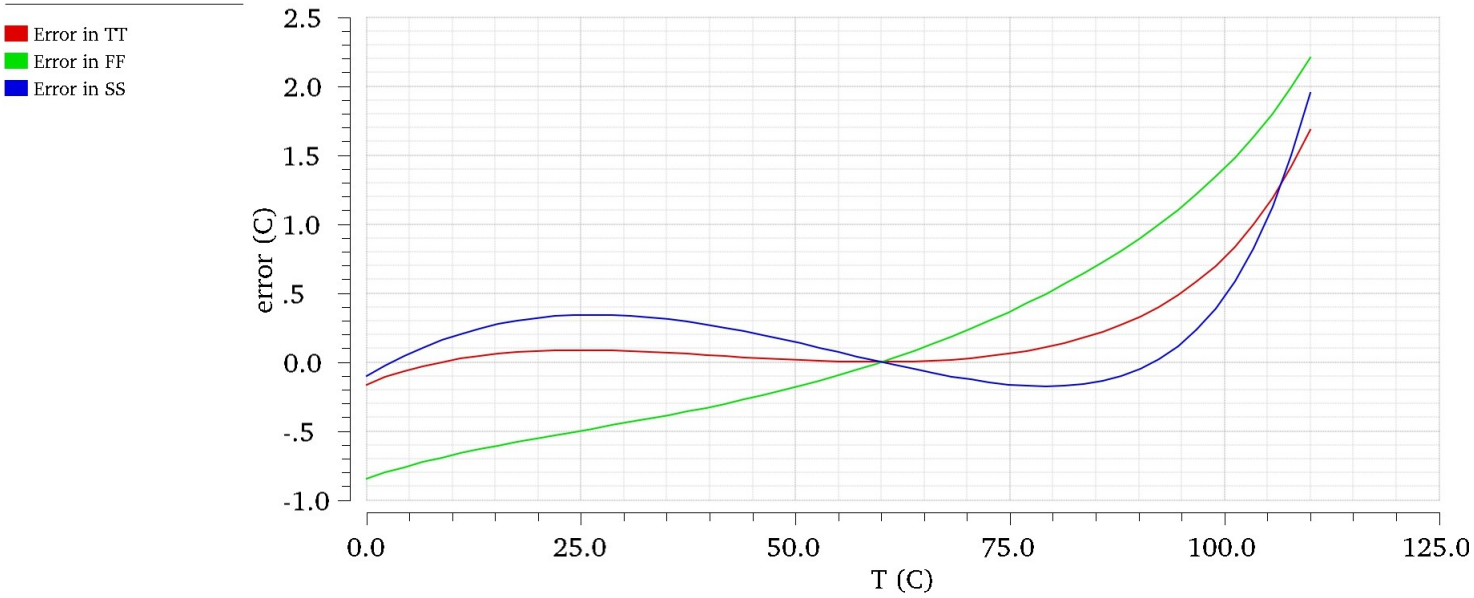

Figure 4.9: The corresponding errors of the designed temperature sensor for TT, SS and FF with temperature range of 0-110 °C.

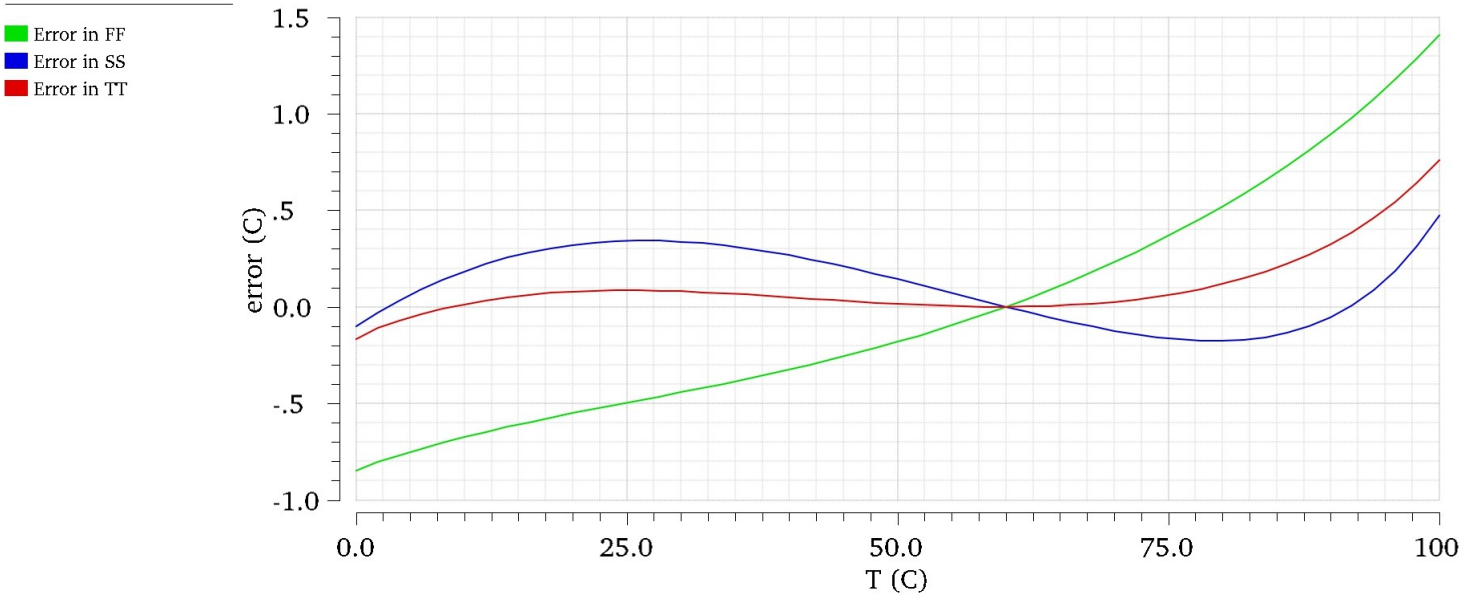

Figure 4.10: The corresponding errors of the designed temperature sensor for TT, SS and FF with temperature range of 0-100 °C.

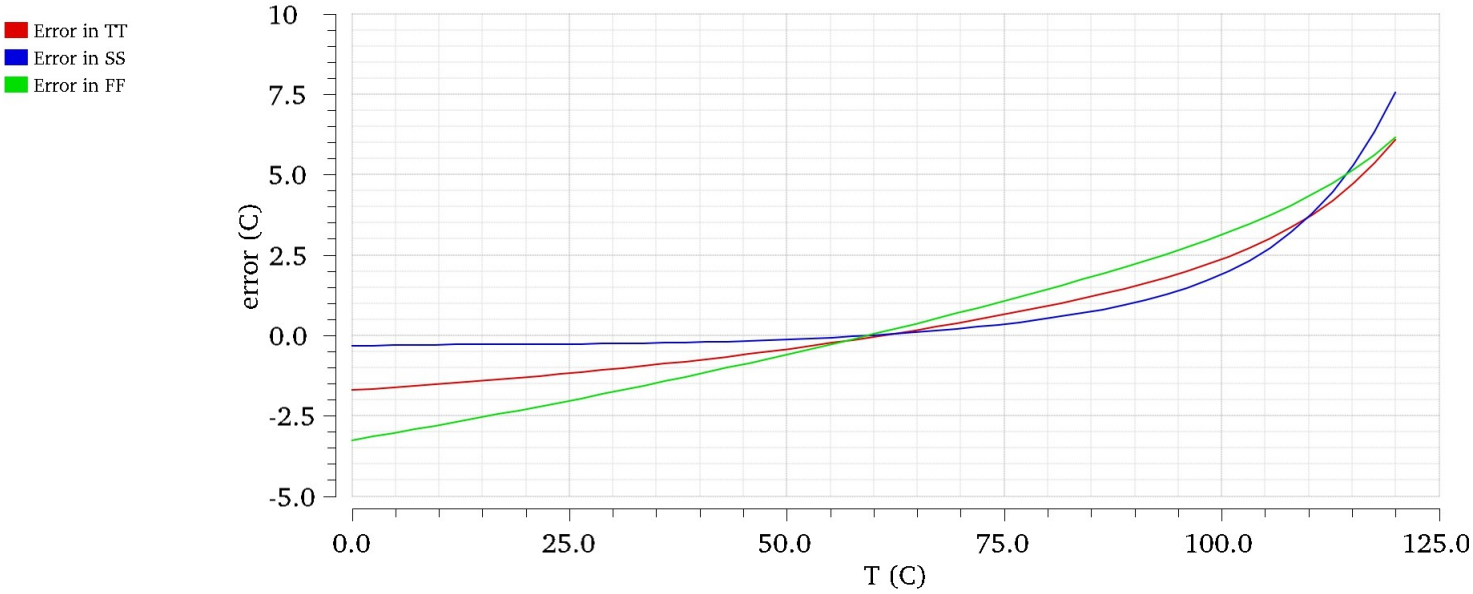

Figure 4.11: The corresponding errors of the designed temperature sensor for TT, SS and FF with run number 1.

laboratory in large scale in different process corners TT, SS and FF respectively.

The figure 4.11 includes the plot of the errors in different process corners from Monte Carlo Simulation with run number of 1. It is seen that TT corner have error in the range of -1.7 to +6.1 °C. On the other hand, the error range of -0.3 to +7.6 C is found for SS corner and that of FF corner was -3.3 to +6.1 °C.

The graph of the errors for different process corners from Monte Carlo Simulation with run number 2 is presented in the figure 4.12. It is found that the error range in TT corner is 0 to +2.4 °C, in SS it is -0.7 to +3.7 °C and in FF -1.2 to +3.6 °C, respectively.

The Monte Carlo Simulation curves with run number 3 for error of the different process corners are given in the figure 4.13. It is observed that the error range for TT is -0.3 to +3.7 °C, for SS it is -0.1 to +5.4 °C and for FF it is -1.1 to +3.5 °C, respectively.

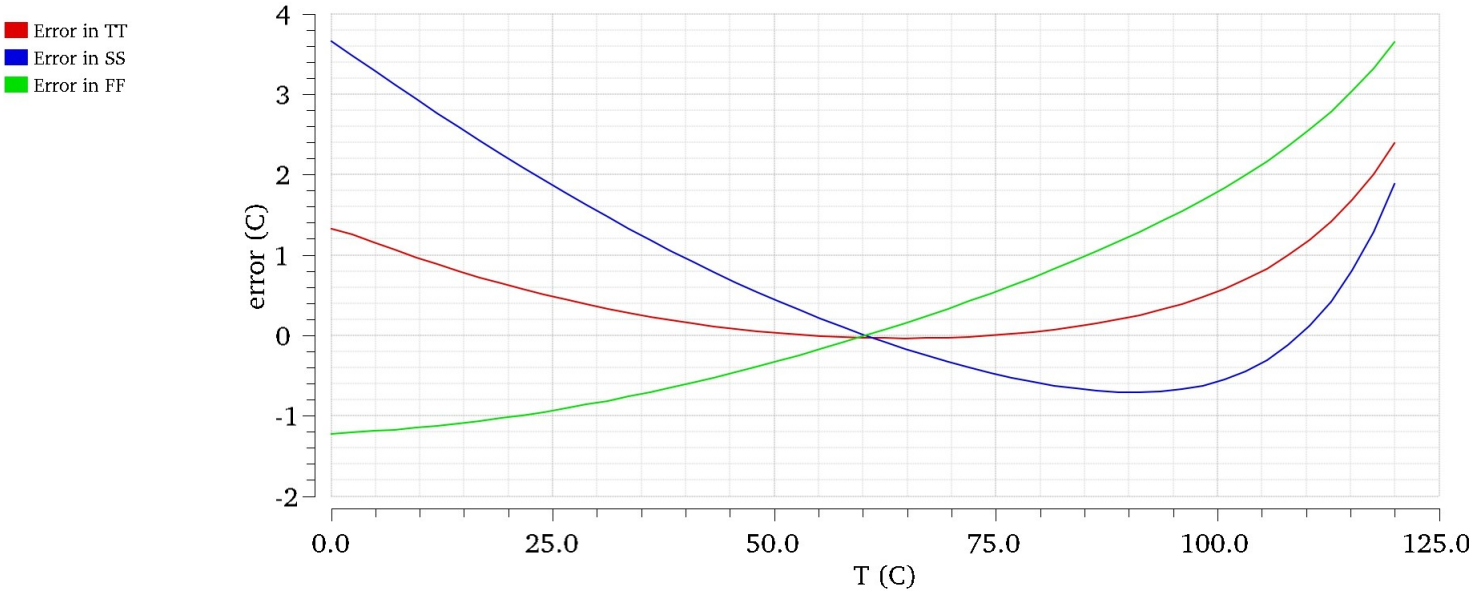

Figure 4.12: The corresponding errors of the designed temperature sensor for TT, SS and FF with run number 2.

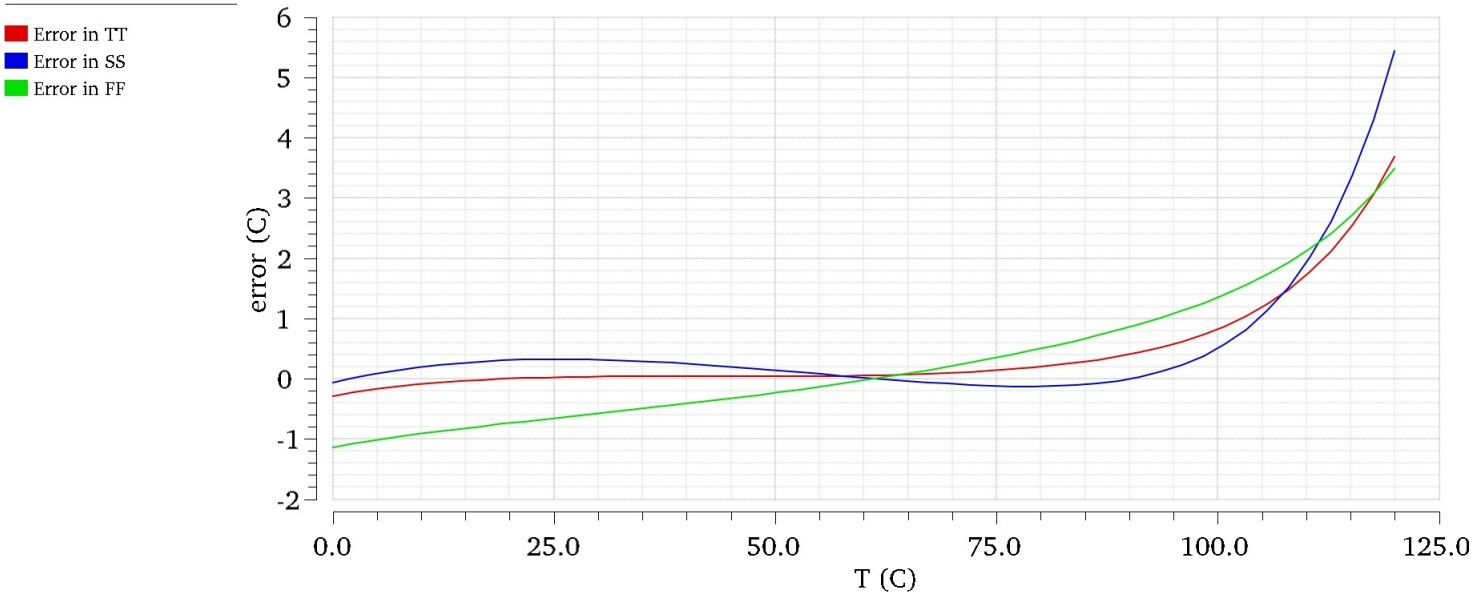

Figure 4.13: The corresponding errors of the designed temperature sensor for TT, SS and FF with run number 3.

Chapter 5

Discussions

This chapter is all about discussing on the designed of the temperature sensor for the ultrasonic probe in general. It is started with comparison of this work with several other related works with focusing on the strengths and weaknesses of the project work. The things that were carried out and not possible to do are also mentioned here. The challenges faced and how they were overcome with learning outcomes are presented in this chapter.

5.1 Comparison with related works

Sensor	Power Supply	Power Consumption	Temperature Range	Inaccuracy Range	Process
[5]	2.2 - 5 V	7 μW	-40 - 120 °C	-1 to +1 °C	—- CMOS
[7]	1 V	150 μW	0 - 60 °C	-5.1 to +3.4 °C	65 nm CMOS
[6]	3.3 V	10 μW	0 - 100 °C	-0.7 to +0.9 °C	0.35 μm CMOS
[8]	1.2 V	288 μW	20 - 120 °C	-0.63 to +1.04 °C	0.13 μm CMOS
[9]	0.5, 1 V	119 nW	-10 - 30 °C	-0.8 to +1 °C	0.18 μm CMOS
[20]	2.7 - 5.5 V	429 μW	-50 - 125 °	-0.5 to +0.5 °C	0.5 μm CMOS
[21]	1 V	220 nW	0 - 100 °C	-1.6 to +3 °C	180 nm CMOS
[22]	1 V	25 μW	50 - 125 °C	-1 to +0.8 °C	90 nm CMOS
[23]	—-	8.6 μW	-55 - 125 °C	-0.4 to +0.4 °C	160 nm CMOS
[18]	0.6 - 2.5 V	7 nW	10 - 120 °C	-2 to +2 °C	180 nm CMOS
This Work	0.6 V	131.2 nW	0 - 120 °C	-3.3 to +7.6 °C	90 nm CMOS

Table 5.1: Comparison of the designed temperature sensor with recent related works

It could be observed from the table 5.1 that this work operates with the lowest supply voltage among all, apart from the work of [9] which operates

with 0.5 V supply voltage, but the difference is only 0.1. One of the significant achievement of this work is the power dissipation, which is lowest among all of them except from the work of [24] on which my circuit design is based on. The work was able to achieve such low power by reducing the drawn current using very large size transistors compared to this work. The comparison of transistors sizes among these two works are illustrated in the table 5.2. The power consumption is also comparable with two other works of [9] and [27], but they achieve this power consumption operating the sensor at the room temperature whereas this work and the work of [24] achieved those power consumption at the maximum temperature of 120 °C. The range of temperature that this sensor work for is also quite wider than most of them, with the exception for the works of [26] and [29], but they have way very high power consumption than this work.

Transistor	W/L (μm/μm) of work [24]	W/L (nm/nm) of this work
M1	1 X (1.5/20)	1 X (180/2400)
M2	10 X (3/3)	10 X (360/360)
M3	4 X (3/3)	4 X (360/360)
M6, M8, M10	1 X (1/3)	1 X (120/360)
M7	3 X (3/3)	3 X (360/360)
M9	4 X (3/3)	4 X (360/360)
M11	28 X (3/3)	14 X (360/360)
M4, M5, M12 - M14	1 X (3/10)	1 X (360/1200)
MC1, MC2	1 X (1/20)	1 X (120/2400)

Table 5.2: Comparison of transistor sizes with the work of [24].

The second noticeable achievement was the use of very small size transistors compared to the work of [24] on which this work was based on. It is designed in 90 nm CMOS process technology which was also used by the work of [28] but did not receive such low power as this work. Moreover, though the work of [7] used process technology of 65 nm, it also have very high power consumption than this work as could be seen from the table 5.1. Apart from power consumption, size also plays a vital role when designing a temperature sensor for portable battery operated devices like the ultrasonic probe. Due to this very small sized transistors, the designed temperature sensor could be constructed in a very small area on the chip of the device only. From the table 5.2, it can be depicted that the transistor sizes are almost 8 times smaller than the work of [24] with M11 multiplier reduced by half (14 from 28). This will result in reduction of the size of the temperature sensor by more than 8 times for sure. Due to the limitation of time converting the schematic to layout and

then post-layout simulation were not possible in order to find accurate area estimation.

The inaccuracy of the designed temperature sensor is quite high among all of the related work as displayed in the table 5.1. This is treated as one of the main drawback of the designed circuit. But, it is seen that when temperature range is reduced, the error in the temperature measurement does reduce also. A decrease in temperature range by 10 °C results in the accuracy to drop below 2°C which is less than the work on which this work is based. Another reason for this error is the noise created by the circuit itself which adds weight in the inaccuracy range. Again, due to time limitation noise reduction work could not be carried out and applied to the circuit to reduce the generated errors. Hence, the inaccuracy of the designed temperature sensor is such high.

5.2 Learning Outcomes

The major outcome of this project is to learn about the different topology of temperature sensors and current mirrors that could be implemented in addition with strengths and weaknesses of each of them. Getting used with the leading analog industrial software Virtuoso along with learning about the Monte Carlo Simulation for looking into the mismatch with different number of fabricated chip numbers was also advantageous. It was beneficial working with the transistors to learn more about them in deep to have a good understanding of their behaviour and hold a more stronger grip on them. Gaining experience in making trade off between power, accuracy and speed for meeting the required specifications to solve the problem statement.

.

Chapter 6

Conclusion

In this thesis work an ultra low power temperature sensor is designed and implemented based on the work from paper [24] in 90 nm CMOS technology process. It is simulated using the Virtuoso software and the outcomes are presented with performance comparison with other related recent works in the table 5.1. The performance of the sensor is highly linear and stable. It is based on the difference between the gate-source voltages of the MOSFET's which is proportional to the absolute temperature in the sub-threshold region. The designed on-chip temperature sensor operates in sub-threshold region with supply voltage of only 600 mV. It covers a wide temperature range from 0-120 °C with inaccuracy of -3.3 to + 7.6 °C over this range. The implemented temperature sensor draws maximum current of 218.66 nA at the highest temperature of 120 °C with mere power consumption of 131.2 nW. Furthermore, when compared to the work of [24], very small sized transistors were uses which were almost 8 times smaller along with reduced number of multiplier for one transistor by half which is illustrated in the table 5.2.

The simulation resulting DC operating points are given in the table 4.1 and corresponding graphs are presented in the figures 4.2 to 4.10. The simulation was carried out in the 3 different process corners namely TT, SS and FF with providing the respective ideal line expressions for the output voltage in terms of measured temperature in the equations 4.1 to 4.4 over these corners. Monte Carlo simulations were also adapted to look into the effect of mismatch in the inaccuracy range for different number of fabricated chips and the graphs are included in the figures 4.11 to 4.13.

6.1 Future Works

First of all, it would be really interesting to go for the noise simulations and look into the noise that is created by the circuit. After that, the required noise

reduction techniques could be look for reducing the noise. By doing so, the accuracy of the designed temperature sensor could be increased by eliminating the added error in the output due to this generated noise. Furthermore, the layout could be done in Virtuoso to observe and investigate about occupying area. Also, it would be fascinating to change the number of pairs of MOSFETs used in the temperature core and notice the change in the output, as by doing so amount of current drawn could be reduce resulting in more lower power consumption. Finally, Monte Carlo simulations could be run for more chip number and detect the error due to mismatch.

.

Bibliography

[1] D. A. M. Arefin, 'A low power and high bandwidth variable gain amplifier for ultrasound application', Department of Electronic Systems, NTNU – Norwegian University of Science and Technology, Project report in TFE4580, Feb. 2020.

[2] M. E. Otey, J. Bi, S. Krishnan, B. Rao, J. Stoeckel, A. Katz, J. Han and S. Parthasarathy, *Automatic view recognition for cardiac ultrasound images*.

[3] Danhua Zhao, S. Zhuang and R. Daigle, 'A commercialized high frequency cmut probe for medical ultrasound imaging', in *2015 IEEE International Ultrasonics Symposium (IUS)*, 2015, pp. 1–4.

[4] S. R. Boyle and R. A. Heald, 'A cmos circuit for real-time chip temperature measurement', in *Proceedings of COMPCON '94*, 1994, pp. 286–291.

[5] A. Bakker and J. H. Huijsing, 'Micropower cmos temperature sensor with digital output', *IEEE Journal of Solid-State Circuits*, vol. 31, no. 7, pp. 933–937, 1996.

[6] Chun-Chi Chen, Wen-Fu Lu, Chin-Chung Tsai and P. Chen, 'A time-to-digital-converter-based cmos smart temperature sensor', in *2005 IEEE International Symposium on Circuits and Systems*, 2005, 560–563 Vol. 1.

[7] C.-C. Chung and C.-R. Yang, 'An autocalibrated all-digital temperature sensor for on-chip thermal monitoring', *IEEE Transactions on Circuits and Systems II: Express Briefs*, vol. 58, pp. 105–109, 2011.

[8] Y. An, K. Ryu, D. Jung, S. Woo and S. Jung, 'An energy efficient time-domain temperature sensor for low-power on-chip thermal management', *IEEE Sensors Journal*, vol. 14, no. 1, pp. 104–110, 2014.

[9] M. K. Law, A. Bermak and H. C. Luong, 'A sub-uw embedded cmos temperature sensor for rfid food monitoring application', *IEEE Journal of Solid-State Circuits*, vol. 45, pp. 1246–1255, 2010.

[10] G. C. M. Meijer, Guijie Wang and F. Fruett, 'Temperature sensors and voltage references implemented in cmos technology', *IEEE Sensors Journal*, vol. 1, no. 3, pp. 225–234, 2001.

[11] G. C. M. Meijer, 'Concepts for bandgap references and voltage measurement systems', in *Analog Circuit Design: Low-Noise, Low-Power, Low-Voltage; Mixed-Mode Design with CAD Tools; Voltage, Current and Time References*, J. H. Huijsing, R. J. van de Plassche and W. M. C. Sansen, Eds. Boston, MA: Springer US, 1996, pp. 243–268, isbn: 978-1-4757-2462-2. doi: 10.1007/978-1-4757-2462-2_13. [Online]. Available: https://doi.org/10.1007/978-1-4757-2462-2_13.

[12] A. Ohte and M. Yamagata, 'A precision silicon transistor thermometer', *IEEE Transactions on Instrumentation and Measurement*, vol. 26, no. 4, pp. 335–341, 1977.

[13] T. C. Verster, 'P–n junction as an ultralinear calculable thermometer', *Electronics Letters*, vol. 4, no. 9, pp. 175–176, 1968.

[14] K. Ueno, T. Asai and Y. Amemiya, 'Low-power temperature-to-frequency converter consisting of subthreshold cmos circuits for integrated smart temperature sensors', *Sensors and Actuators A: Physical*, vol. 165, no. 1, pp. 132–137, 2011, Transducers 2009, issn: 0924-4247. doi: https://doi.org/10.1016/j.sna.2010.03.030. [Online]. Available: http://www.sciencedirect.com/science/article/pii/S0924424710001354.

[15] Y. Taur and T. H. Ning, *Fundamentals of Modern VLSI Devices*, 2nd ed. Cambridge University Press, 2009. doi: 10.1017/CBO9781139195065.

[16] T. Carusone, D. Johns and K. Martin, *Analog Integrated Circuit Design, 2nd Edition*. Wiley, 2011, isbn: 9781118213735. [Online]. Available: https://books.google.no/books?id=GeobAAAAQBAJ.

[17] D. Ma, C. Zheng, H. Chao and M. Koen, 'Integrated low-power cmfb-free variable-gain amplifier for ultrasound diagnostic applications', *Analog Integrated Circuits and Signal Processing*, vol. 61, pp. 171–179, Nov. 2009. doi: 10.1007/s10470-009-9296-8.

[18] A. Sahafi, J. Sobhi and Z. daie koozehkanani, 'Nano watt cmos temperature sensor', *Analog Integrated Circuits and Signal Processing*, vol. 75, Jun. 2013. doi: 10.1007/s10470-013-0046-6.

[19] M. Hasanuzzaman, S. K. Islam and L. M. Tolbert, 'Effects of temperature variation (300–600 k) in mosfet modeling in 6h–silicon carbide', *Solid-State Electronics*, vol. 48, no. 1, pp. 125–132, 2004, issn: 0038-1101. doi: https://doi.org/10.1016/S0038-1101(03)00293-4. [Online]. Available: http://www.sciencedirect.com/science/article/pii/S0038110103002934.

[20] M. A. P. Pertijs, A. Niederkorn, Xu Ma, B. McKillop, A. Bakker and J. H. Huijsing, 'A cmos smart temperature sensor with a 3/spl sigma/ inaccuracy of /spl plusmn/0.5/spl deg/c from -50/spl deg/c to 120/spl deg/c', *IEEE Journal of Solid-State Circuits*, vol. 40, no. 2, pp. 454–461, 2005.

[21] Yu-Shiang Lin, D. Sylvester and D. Blaauw, 'An ultra low power 1v, 220nw temperature sensor for passive wireless applications', in *2008 IEEE Custom Integrated Circuits Conference*, 2008, pp. 507–510.

[22] M. Sasaki, M. Ikeda and K. Asada, 'A temperature sensor with an inaccuracy of $-1/+0.8$ ° c using 90-nm 1-v cmos for online thermal monitoring of vlsi circuits', *IEEE Transactions on Semiconductor Manufacturing*, vol. 21, no. 2, pp. 201–208, 2008.

[23] K. Souri, Y. Chae, Y. Ponomarev and K. A. A. Makinwa, 'A precision dtmost-based temperature sensor', in *2011 Proceedings of the ESSCIRC (ESSCIRC)*, 2011, pp. 279–282.